



HAL
open science

Analysis through thermogravimetric analyses of the impact of torrefaction processes performed under a non-oxidative atmosphere on hydrolysis lignin samples

Alain Brillard, Gwenaëlle Trouve, P. Maryandyshev, Damaris Kehrli, V. Lyubov, Jean-Francois Brillhac

► To cite this version:

Alain Brillard, Gwenaëlle Trouve, P. Maryandyshev, Damaris Kehrli, V. Lyubov, et al.. Analysis through thermogravimetric analyses of the impact of torrefaction processes performed under a non-oxidative atmosphere on hydrolysis lignin samples. *Fuel*, 2019, 260, pp.116261. 10.1016/j.fuel.2019.116261 . hal-03278798

HAL Id: hal-03278798

<https://hal.science/hal-03278798>

Submitted on 21 Dec 2021

HAL is a multi-disciplinary open access archive for the deposit and dissemination of scientific research documents, whether they are published or not. The documents may come from teaching and research institutions in France or abroad, or from public or private research centers.

L'archive ouverte pluridisciplinaire **HAL**, est destinée au dépôt et à la diffusion de documents scientifiques de niveau recherche, publiés ou non, émanant des établissements d'enseignement et de recherche français ou étrangers, des laboratoires publics ou privés.



Distributed under a Creative Commons Attribution - NonCommercial 4.0 International License

1 **Analysis through thermogravimetric analyses of the impact of torrefaction**
2 **processes performed under a non-oxidative atmosphere on hydrolysis lignin samples**

3

4 **A. Brillard^{a1}, G. Trouvé^a, P. Maryandyshev^b, D. Kehrlia, V. Lyubov^b, J.-F. Brilhac^a**

5

6 ^a *Laboratoire Gestion des Risques et Environnement (EA 2334), Institut de Recherche Jean-*
7 *Baptiste Donnet, Université de Haute-Alsace, 3bis, rue Alfred Werner F-68093 Mulhouse Cedex,*
8 *France*

9 ^b *Department of Industrial Power Engineering, Institute of Energy and Transport, Northern*
10 *(Arctic) Federal University named after M.V. Lomonosov, 163002, Northern Dvina Embankment*
11 *17, Arkhangelsk, Russian Federation.*

12

13 **Abstract**

14 Hydrolysis lignin samples were torrefied in a fixed bed reactor under a nitrogen flow, under four
15 different isothermal temperatures (225, 250, 275 or 300 °C) and during 30 or 60 minutes. The
16 impact of such torrefaction conditions on the hydrolysis lignin samples was analyzed through
17 thermogravimetric analyses performed under non-oxidative or oxidative atmospheres and under
18 a heating rate of 5 °C/min. The thermogravimetric profile and the reactivity of the raw and
19 torrefied samples were compared. The optimal values of the kinetic parameters were determined
20 using the EIPR model, first determining the number of constituents to be considered, then their
21 proportions applying Van Soest's protocol to the raw material and adjusting them for the
22 torrefied samples. These values of the kinetic parameters were validated through observations of
23 the experimental and simulated mass and mass rate curves and computations of the maximal

¹ *Corresponding author.
Email-address: Alain.Brillard@uha.fr (A. Brillard)

24 difference between these curves. The values of the kinetic parameters did not significantly vary
25 with the isothermal temperature or with the torrefaction residence time.

26

27 **Keywords:** Hydrolysis lignin; non-oxidative torrefaction process; thermogravimetric analysis;
28 EIPR model; optimal kinetic parameters; optimal torrefaction conditions

29

30 **1. Introduction**

31 Replacing fossil fuels with renewable materials or by-products from industry or even associating
32 both is a very interesting perspective for energy production. For example, the use of biomass as
33 combustible first presents interesting characteristics for energy production through combustion,
34 gasification, liquefaction and pyrolysis processes. Then the use of biomass or of their by-
35 products (e.g. ethanol, methane, bio-oil and char) does not further lead to an increase in the
36 overall CO₂ balance, even if the CO₂ which was absorbed by the plants and trees from the
37 atmosphere through the photosynthesis process during their growth is released through the
38 degradation process [1]. Integrating torrefied biomass into coal-fired power plants could further
39 potentially lower the SO_x and net CO₂ emissions resulting from electricity generation [2].

40 Hydrolysis lignin (HL) is a by-product of technological cycles concerning the production of fuels
41 and chemicals, through either a percolation hydrolysis of wood using dilute H₂SO₄ at elevated
42 temperatures and pressures (Scholler process) or a low-temperature hydrolysis of wood using
43 concentrated HCl (Bergius process) [3]. Wood hydrolysis plants were mainly built in the former
44 USSR, Bulgaria, China and Korea. All these plants produced substantial amounts of hydrolysis
45 lignin, at most 1.5 million tons each year by the 1980's [3-4]. The Russian hydrolysis industry
46 collapsed in the first decade of the 2000s [4]. But there still exist huge dumps of hydrolysis
47 lignin in Russia and in countries of the Eastern Block [4].

48 HL is mainly composed of lignin, balanced with unreacted cellulose, mono- and oligo-
49 saccharides [5]. According to its chemical content, HL is close to carbohydrates, but it differs

50 from them with higher carbon contents. The elemental analysis of HL depends on the
51 technological ethanol cycle. HL samples present differences depending on the dump where they
52 are collected [4]. But they are all characterized by high amounts of carbon and of lignin and by a
53 low percentage of ash. HL is a highly reactive fuel and has a high ignition ability. HL should
54 thus be considered as a valuable renewable fuel for energy production.

55 During a torrefaction process, sometimes also called “mild pyrolysis”, the material is heated up
56 to an isothermal temperature under low heating rates (less than 50 °C/min), then maintained at
57 the chosen isothermal temperature for a residence time which is usually taken less than 60
58 minutes. The torrefaction process is usually performed under an inert atmosphere. The result of
59 this torrefaction process is a dark material whose chemical and physical properties slightly differ
60 from that of the original material [6-13]. For example, the torrefaction process increases the
61 heating values and the energy density of the material [6], among other works. During the
62 torrefaction process, the moisture content and volatile matter with higher oxygen content are
63 removed and hydroxyl groups are reduced (which make the hydrogen bonds due to the moisture
64 content). Small mass losses may be observed during this torrefaction process which leads to the
65 production of a hydrophobic fuel with higher density [14]. The volatiles which are emitted
66 during the pyrolysis process are mainly issued from the hemicellulose and cellulose
67 degradations, which reduces the energy costs for the milling of the torrefied wood, as
68 hemicellulose fills in the wood cell structure, thus reinforcing its integrity [15-17]. Laboratory
69 and industrial investigations prove that combining torrefaction and pelletization processes allows
70 producing hydrophobic and ecologically clean fuels with increased calorific value and density.
71 This finally allows cheaper transportation and use conditions [18-22]. The char which is
72 produced through a torrefaction process can also be milled together with traditional coals in the
73 existing mills, while the milling of classical pellets needs the modernization of fuel preparation
74 and handling systems, which leads to higher operational costs [23].

75 The impact of torrefaction processes on the thermal degradation of different materials was
76 analyzed through thermogravimetric analyses in many works even recently. In [24], the authors
77 analyzed the impact of torrefaction operating conditions on the thermal degradation of olive tree
78 pruning. The torrefaction experiments were performed at 200 or 300 °C and residence times of
79 10 and 60 minutes, using an inert atmosphere (nitrogen). The authors used a parallel reaction
80 scheme to determine the kinetic parameters associated to the different components of the
81 material. In [25], the authors analyzed the influence of torrefaction processes on hybrid variety
82 oil palm plantation (*Elaeis guineensis* and *Elaeis oleifera*). The torrefaction experiments were
83 performed at 220, 250 or 270 °C and during residence times of 30 and 60 minutes, under an inert
84 atmosphere (nitrogen). The authors used a formal pseudo-components parallel independent
85 reactions kinetic model to derive the optimal values of the kinetic parameters. In [26], the
86 authors analyzed the impact of a torrefaction process performed on Norwegian spruce stump
87 chips through a thermogravimetric analysis. They used a distributed activation energy model
88 (DAEM) model to determine the optimal values of the kinetic parameters of the raw and
89 torrefied materials. The authors also compared these values of the kinetic parameters with that
90 returned by the Ozawa method. In the review [27], the authors collected results from different
91 studies and concerning the impact of different experimental parameters when performing
92 torrefaction processes on agricultural or food waste (lignocellulosic materials) and on non-
93 lignocellulosic materials. They especially discussed the properties of the torrefied materials in
94 terms of grindability, hydrophobicity and combustibility. In [28], the authors collected results
95 from the literature and concerning the impact of torrefaction processes performed on different
96 woody and non-woody materials, under different isothermal temperatures (between 200 and 300
97 °C) and during 30 or 60 minutes. In the review [29], the authors analyzed the results from the
98 literature and concerning the torrefaction of different materials in an inert atmosphere, at
99 isothermal temperatures less than 300 °C and under residence times mainly less than 60 minutes.
100 They presented the results of kinetic modeling applied to these materials and based on different

101 methods or models. They analyzed the impact of torrefaction conditions on the density of the
102 torrefied materials. See also the references in the reviews [27-29].

103 To our knowledge, the impact of torrefaction processes on HL samples was never analyzed. The
104 aim of this work was thus to investigate the impact of different but classical torrefaction
105 processes performed on HL samples on their thermogravimetric profile and on their reactivity.
106 HL samples were collected in the Onega dump in Arkhangelsk oblast, Russian Federation.
107 Torrefaction experiments were performed in a fixed bed reactor under nitrogen, under four
108 different isothermal temperatures (225, 250, 275, 300 °C) and during two different residence
109 times (30 or 60 minutes). Thermogravimetric analyses were then performed on the raw and
110 torrefied samples from ambient temperature up to 900 °C under a heating rate of 5 °C/min and
111 under non-oxidative or oxidative atmospheres. The Extended Independent Reaction (EIPR)
112 model was used to determine the optimal values of the kinetic parameters associated to the
113 thermal degradations of these different samples. This model was already used in previous studies
114 to simulate the thermal degradations of different materials. It is essentially based on the
115 degradations of the different constituents of the material (at least hemicellulose, cellulose, lignin,
116 plus char if the degradation occurs under an oxidative atmosphere), which are supposed to occur
117 in an almost independent way. The number of constituents to be taken into account for the raw
118 and torrefied HL samples was taken equal to four (hemicellulose, cellulose and two stages of the
119 lignin degradation), because of the presence of peaks, shoulders and tails on the mass rate
120 curves. The very high proportion of lignin in HL samples (around 2/3 in the raw material) may in
121 part explain the shape of the mass rate curves, the lignin pyrolysis being further a complex
122 process as many chemical reactions occur [30,31]. The proportions of hemicellulose, cellulose
123 and lignin were determined applying Van Soest's protocol, as described in [32], to the raw
124 material (for which a sufficient amount was available). These proportions were adjusted for the
125 torrefied samples observing their mass rate curves. In the EIPR model with four constituents, the
126 extractives were added to the hemicellulose and cellulose constituents (half for each). The

127 optimal values of the kinetic parameters returned by the EIPR model were used to draw
128 simulated mass and mass rate curves. The maximal difference between the experimental and
129 simulated mass rate curves was computed for each sample to validate the optimal values of the
130 kinetic parameters returned by the EIPR model. The optimal values of the kinetic parameters
131 returned by the EIPR model for the raw and the torrefied materials were finally compared and
132 they did not vary in a significant way, except for the sample torrefied at 300 °C. The torrefaction
133 processes considered in the present study did not degrade in a significant way the HL samples.
134 But they reduced their moisture content and they increased their carbon content and the calorific
135 value.

136

137 **2. Materials and methods**

138 *2.1 Hydrolysis lignin characterizations*

139 Hydrolysis lignin (HL) was kindly provided by the Bionet company who produces HL pellets
140 from the Onega lignin dump, located in the Arkhangelsk region, North-East of the Russian
141 Federation. The current amount of available HL was evaluated at 3.0×10^6 tons in this dump [4].
142 Before their use in the experiments, the samples were ground in a ball mill (Retzsch PM 200)
143 and sieved on a Retzsch AS 200 Control analyzer to a particle size distribution 500–1000
144 micrometers.

145 The C, H, O, N and S fractions of raw HL samples were determined on an analyzer EuroVector
146 EA-300. The biochemical composition of raw HL was determined according to Van Soest's
147 protocol described in [32]. Proximate analyses were performed by thermogravimetry according
148 to the German standard DIN 51734 on "Testing of solid mineral fuels - Proximate analysis and
149 calculation of fixed carbon". The Higher Heating Values (HHV) of raw and torrefied materials
150 were measured using a calorimeter IKA C 2000 Basic version 2. The Lower Heating Value
151 (LHV) of each sample was then deduced from its HHV by calculations taking into account the
152 proximate and ultimate analyses, according to the formula:

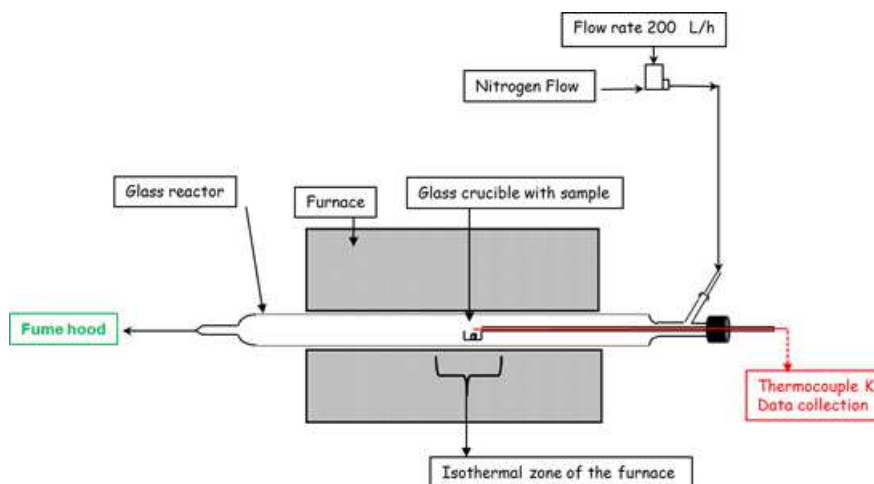
153
$$LHV = HHV - L_v \left(\frac{M}{100} + \frac{M_{H_2O}H}{200M_H} \right), \quad (1)$$

154 where $L_v=2486$ kJ/kg is the latent heat of water vaporization at 273 K, M is the moisture content
 155 (%), $M_{H_2O}=18$ g/mol is the molar mass of water, $M_H=1$ g/mol is the molar mass of hydrogen and
 156 H is the percentage of hydrogen of the sample and given in Table 1 below.

157

158 *2.2 Torrefaction experiments*

159 For the different torrefaction experiments, samples with an initial mass of 1.01 ± 0.02 g were
 160 introduced in the crucible of a horizontal fixed bed reactor whose scheme is presented in Fig. 1.



161

162 **Fig. 1.** Scheme of the experimental horizontal fixed bed reactor used for the torrefaction
 163 processes.

164

165 The fixed bed reactor was heated with electrical resistances with a heating rate of 20 °C/min to
 166 reach the isothermal temperature of 225, 250, 275 or 300 °C. Then the sample was kept under
 167 this isothermal temperature during 30 or 60 minutes. The nitrogen flow was fixed at 200 l/h
 168 under standard temperature and pressure conditions (273K and 101,325 Pa). The overall length
 169 of the fixed bed reactor was 1m. The dimensions of the glass crucible were 55 mm length, 28
 170 mm width and 25 mm height. The thermocouple type K was placed just above the sample (4-5
 171 mm above).

172 Each torrefaction experiment was repeated between seven and nine times to reduce possible
173 deviations.

174

175 *2.3 Thermogravimetric analyses*

176 Thermogravimetric analyses were performed on the raw and torrefied HL samples in a
177 thermobalance TA Instruments Q500. The samples were submitted to non-oxidative (nitrogen)
178 or oxidative (synthetic air: 10% O₂ and balance nitrogen) atmospheres under a flow rate of 6 l/h
179 under standard temperature and pressure conditions (273K and 101,325 Pa). They were heated
180 from ambient temperature to 900 °C under a heating rate equal to 5 °C/min. The purpose of these
181 thermogravimetric analyses is to evaluate the impact of the torrefaction conditions on the thermal
182 degradation of HL samples and on their reactivity under such non-oxidative or oxidative
183 atmospheres. For each experiment, around 10 mg of material were placed in the crucible of the
184 thermobalance. Thermogravimetric experiments were repeated at least three times for each raw
185 or torrefied sample with good repeatability.

186

187 *2.4 Kinetic modeling through the EIPR model in the case of a non-oxidative atmosphere*

188 The EIPR model is especially dedicated to the simulation of the thermal degradation of a
189 lignocellulosic material [33-36]. It indeed considers the thermal degradation of its constituents,
190 namely at least hemicellulose, cellulose, lignin, plus the char structure if the thermal degradation
191 occurs under an oxidative atmosphere. The EIPR model assumes that the thermal degradations of
192 these constituents occur in an independent way, but possibly in superimposing temperature
193 ranges.

194 In the case of a non-oxidative atmosphere, the EIPR model consists in a set of ordinary
195 differential equations, whose number I is equal to the number of constituents to be taken into
196 account in the material, each equation describing the evolution of the mass of volatiles which are
197 emitted from a constituent of the material. Each ordinary differential equation is written as:

198
$$\frac{dm_{vol,i}^e}{dt}(t) = k_i(T(t)) \left(m_i(0) - m_{vol,i}^e(t) \right), i = 1, \dots, I, \quad (2)$$

199 where $m_{vol,i}^e(t)$ is the mass of volatiles emitted by the constituent i of the sample ($i=1, \dots, I$),
 200 $m_i(0)$ is the initial mass of the constituent i which may be computed as a fraction of the overall
 201 mass of the sample: $m_i(0) = c_i m(0)$, $T(t)$ is the temperature (expressed in K) at time t in the
 202 sample and which evolves with respect to the time parameter t with a constant rate: $T(t) = at +$
 203 T_0 .

204 In the right-hand side of the equation (2), a first-order reaction function with respect to the extent
 205 of conversion α is here considered: $f(\alpha) = 1 - \alpha$, whatever the constituent of the each sample.

206 In the right-hand side of the equation (1), the kinetic constant $k_i(T(t))$ obeys an Arrhenius law:

207 $k_i(T(t)) = A_i \exp\left(-\frac{Ea_i}{RT(t)}\right)$, where A_i (resp. Ea_i) is the pre-exponential factor (resp. the

208 activation energy) for the constituent i and R is the ideal gas constant equal to 8.314 J/mol K. In

209 the present study, the system of differential equations (2) is solved with the Scilab software

210 (routine 'ode'), first with initial guesses of the kinetic parameters. The optimal values of the

211 kinetic parameters are then obtained using the routine 'datafit' of Scilab that is minimizing with

212 respect to these kinetic parameters the objective function expressed as:

213
$$\sum_{j=1}^J \left(\left(\frac{dm_{vol,i}^e}{dt} \right)_{exp}(t_j) \left(\left(\frac{dm_{vol,i}^e}{dt} \right)_{exp}(t_j) - \left(\frac{dm_{vol,i}^e}{dt} \right)_{sim}(t_j) \right) \right)^2, \quad (3)$$

214 where $\left(\frac{dm_{vol,i}^e}{dt} \right)_{exp}(t_j)$ is the experimental mass rate at time t_j and $\left(\frac{dm_{vol,i}^e}{dt} \right)_{sim}(t_j)$ is the

215 simulated mass rate at time t_j , as deduced from the resolution of (2). Around 200 points t_j are

216 chosen which are regularly distributed along the overall duration of the experiment to reduce the

217 computation time.

218 Once the optimal values of the kinetic parameters have been determined, it is possible to solve

219 the system (2) to obtain the simulated sample mass and mass rate according to:

220
$$m(t) = m(0) - \sum_{i=1}^I m_{vol,i}^e(t), \quad (4)$$

221
$$\frac{dm}{dt}(t) = \sum_{i=1}^I \frac{dm_{vol,i}^e(t)}{dt}. \quad (5)$$

222

223 *2.5 Kinetic modeling through the EIPR model in the case of an oxidative atmosphere*

224 Under an oxidative atmosphere, the devolatilization stages of the material surely occur. But the
 225 char structure is also degraded. One could consider this char structure as a further constituent and
 226 thus add a further equation in the model presented in the previous section concerning the EIPR
 227 model in the case of a non-oxidative atmosphere. But the EIPR model instead consider that the
 228 main constituents of the material (hemicellulose, cellulose and lignin) lead to both the emission
 229 of volatiles and to the apparition of the char structure once the volatiles are being emitted from
 230 these constituents, this char structure being degraded at higher temperatures. The proportion of
 231 volatiles to be emitted from the constituent i is denoted as $\tau_{vol,i}$. The complement of $\tau_{vol,i}$ to 1
 232 represents the proportion of char structure which appears from the constituent i during the
 233 devolatilization stage and which will be degraded during the combustion stage.

234 Under an oxidative atmosphere, the EIPR model first simulates the evolution of the mass of
 235 volatiles which are emitted from the constituent i of the material with respect to time according
 236 to the ordinary differential equation:

237
$$\frac{dm_{vol,i}^e}{dt}(t) = k_i(T(t)) \left(m_i(0) - \frac{m_{vol,i}^e(t)}{\tau_{vol,i}} \right), i = 1, \dots, I, \quad (6)$$

238 where $m_{vol,i}^e(t)$ is the mass of volatiles emitted by the constituent i of the sample ($i=1, \dots, I$),
 239 $m_i(0)$ is the initial mass of the constituent i , which may be computed as a fraction of the overall
 240 mass of the sample: $m_i(0) = c_i m(0)$, $T(t)$ is the temperature at time t in the sample (expressed
 241 in K) and which evolves with respect to the time parameter t with a constant rate: $T(t) = at +$
 242 T_0 and $\tau_{vol,i}$ is the fraction of volatiles contained in the constituent I and which will be emitted

243 during the devolatilization stage, as previously exposed. This fraction $\tau_{vol,i}$, has to be determined
 244 for each HL sample and for each constituent which is not an easy task. In the present study, this
 245 fraction has been estimated observing the mass rate curves obtained from the thermal
 246 degradation of each material under an oxidative atmosphere. The presence of the fraction $\tau_{vol,i}$,
 247 of volatiles emitted by the constituent i of the sample is the unique difference between the
 248 equations (4) and (6).

249 In the above equation (6), the kinetic constant $k_i(T(t))$ obeys an Arrhenius law: $k_i(T(t)) =$
 250 $A_i \exp(-Ea_i/RT(t))$, where A_i (resp. Ea_i) is the pre-exponential factor (resp. the activation
 251 energy) for the devolatilization of the constituent i .

252 The evolution with respect to time of the mass $m_{char,i}^c$ of char which appears during the
 253 devolatilization of the constituent i is described according to the ordinary differential equation:

$$254 \quad \frac{dm_{char,i}^c}{dt}(t) = k_{comb}(T(t)) \left(\frac{1 - \tau_{vol,i}}{\tau_{vol,i}} m_{vol,i}^e(t) - m_{char,i}^c(t) \right) P_{O_2}, \quad (7)$$

255 where the kinetic constant $k_{comb}(T)$ obeys an Arrhenius law: $k_{comb}(T) =$
 256 $A_{comb} \exp(-Ea_{comb}/RT)$ and where P_{O_2} is the oxygen pressure which is constant during the
 257 experiment ($P_{O_2} = 2.1 \times 10^4$ Pa).

258 The system (6)-(7) is solved using the routine 'ode' of Scilab software, first with initial guesses
 259 of the kinetic parameters. The optimal values of the kinetic parameters are obtained minimizing
 260 with the routine 'datafit' of Scilab the objective function defined as:

$$261 \quad \sum_{j=1}^J \left(\left(\left(\frac{dm_{vol,i}^e}{dt} \right)_{exp}(t_j) + \left(\frac{dm_{char,i}^c}{dt} \right)_{exp}(t_j) \right) \left(\left(\frac{dm_{vol,i}^e}{dt} \right)_{exp}(t_j) + \left(\frac{dm_{char,i}^c}{dt} \right)_{exp}(t_j) \right) \right. \\ \left. - \left(\frac{dm_{vol,i}^e}{dt} \right)_{sim}(t_j) - \left(\frac{dm_{char,i}^c}{dt} \right)_{sim}(t_j) \right)^2, \quad (8)$$

263 where $\left(\frac{dm_{vol,i}^e}{dt}\right)_{exp}(t_j)$ is the experimental volatile mass rate at time t_j , $\left(\frac{dm_{char,i}^c}{dt}\right)_{exp}(t_j)$ is the
 264 experimental char mass rate at time t_j , $\left(\frac{dm_{vol,i}^e}{dt}\right)_{sim}(t_j)$ is the simulated volatile mass rate at time
 265 t_j and $\left(\frac{dm_{char,i}^c}{dt}\right)_{sim}(t_j)$ is the simulated char mass rate at time t_j , as deduced from the resolution
 266 of the system (4)-(5). Around 200 points t_j are chosen which are regularly distributed along the
 267 overall duration of the experiment to reduce the computation time.
 268 Again, only a first-order reaction function is here considered: $f(\alpha) = 1 - \alpha$, whatever the
 269 constituent of the each raw or torrefied sample.

270 Once the optimal values of the kinetic parameters have been determined, it is possible to solve
 271 the system (6)-(7) to obtain the simulated sample mass and mass rate according to:

$$272 \quad m(t) = m(0) - \sum_{i=1}^I m_{vol,i}^e(t) - \sum_{i=1}^I m_{char,i}^c(t), \quad (9)$$

$$273 \quad \frac{dm}{dt}(t) = \sum_{i=1}^I \frac{dm_{vol,i}^e}{dt}(t) - \sum_{i=1}^I \frac{dm_{char,i}^c}{dt}(t), \quad (10)$$

274 from which it is possible to draw the simulated mass and mass rate curves. It is also possible to
 275 compute the maximal difference between the experimental and simulated mass rate curves.
 276 When using the EIPR model, the simulated mass and mass rate curves obtained for different
 277 materials have been proved to be in good agreement with the experimental ones [26,33-36], the
 278 maximal difference between the experimental and simulated mass rate curves being sufficiently
 279 small with respect to the maximal mass rate to validate the values of the kinetic parameters
 280 returned by the EIPR model.

281 Observe that the equations of the EIPR model are close to that of the DAEM model [36].

282

283 **3. Results and discussion**

284 *3.1 Thermal and chemical characterizations*

285 Table 1 gathers the thermal and chemical characterizations of the raw and torrefied HL samples.

286

287 **Table 1**

288 Proximate, ultimate analysis, Lower Heating Value (LHV) and carbon enrichment ratio of the
 289 raw and torrefied HL samples under the different experimental conditions.

%	Raw	225 °C	250 °C	275 °C	300 °C	225 °C	250 °C	275 °C	300 °C
		30 min	30 min	30 min	30 min	60 min	60 min	60 min	60 min
Volatile matter ^a	65.8	62.9	62.6	59.3	56.9	62.6	62.2	58.4	56.6
Fixed carbon ^a	34.2	37.1	37.4	40.7	43.1	37.4	37.8	41.6	43.4
Moisture ^b	5.1	2.4	2.4	2.2	2.1	2.1	2.4	2.2	2.1
Ash ^b	4.2	7.7	8.3	8.3	9.2	7.8	8.3	8.4	9.8
C ^a	59.5	60.0	60.6	62.7	67.8	60.3	61.2	63.0	68.3
H ^a	6.5	6.1	5.9	5.7	5.4	6.0	5.8	5.5	5.2
O ^a	33.7	33.5	32.2	31.3	26.5	33.3	32.7	31.2	26.2
LHV (MJ/kg) ^a	21.6	23.1	23.7	24.0	24.5	23.5	24.1	24.8	25.3
Carbon enrichment ratio	1.00	1.20	1.21	1.31	1.39	1.21	1.22	1.34	1.40

290 ^aon dry and ash free basis; ^bon dry basis.

291

292 The Fixed Carbon percentage was obtained by difference for each sample. It increases with the
 293 isothermal temperature, whatever the residence time. The increase is equal to 26% for a
 294 residence time of 30 minutes and to 27% for a residence time of 60 minutes. Consequently, the
 295 percentage of volatiles decreases with the isothermal temperature. The moisture content
 296 decreases with the isothermal temperature being divided by 2.5 from the raw material. The ash
 297 content increases by a factor 2.2 or 2.3, because HL loses other parts of its constituents during
 298 the torrefaction process.

299 HL samples collected in different regions of the Russian Federation and of countries from the
 300 Eastern Block have been analyzed in [4], among which that of Onega dump. The hydrolysis

301 lignin from Omega dump contains the lowest ash percentage among those which have been
302 tested.

303 The N fraction of the raw or torrefied material remains close to 0.2-0.3% and that of S is below
304 the detection limit equal to 0.1%. The corresponding values are not indicated in Table 1.

305 The C content of torrefied HL samples increases while the O content decreases when the
306 isothermal temperature increases and also when the residence time increases.

307 The carbon enrichment ratio is computed for each sample as the ratio between the C content of
308 this sample and that of the raw material. It increases with the isothermal temperature and it also
309 slightly increases with the residence time.

310 In [34], the authors compared the impact of wet and dry torrefaction on microalgal biomass.
311 They also observed similar trends with respect to the isothermal temperature (taken equal to 200,
312 250 or 300 °C) and to the residence time (taken equal to 15, 30 45 or 60 minutes).

313 The torrefaction process increases the LHV values from that of the raw HL material.

314 The biochemical composition of the raw sample was determined according to Van Soest's
315 protocol [32]. The mass proportions of the constituents of the raw material are as follows:
316 extractives (15.2%), hemicellulose (2.3%), cellulose (15.6%) and lignin (66.9%). HL samples
317 also contain light molecules as extractives. Hemicellulose is present as traces and cellulose
318 mainly consists of sugar polymers. The lignin polymer is the main constituent of HL,
319 approximately representing 2/3 in mass of the material.

320 Torrefaction and energy yields have been computed for each sample. As above-indicated, for
321 each torrefaction condition, between seven and nine experiments have been performed, each of
322 them with approximately 1g of hydrolysis lignin. To remove the dependence of the yields with
323 respect to the initial mass, this initial mass has been normalized to 1g in the computations. The
324 normalized final mass has been obtained as the ratio between the final mass and the original
325 mass. The torrefaction yield is computed as:

326
$$\tau_s = \frac{m_{final}}{m_{init}}, \quad (7)$$

327 where m_{final} is the final (after torrefaction) mass of the sample (kg) and m_{init} is the initial
 328 (before torrefaction) mass of the sample (kg). The energy yield is computed as:

$$329 \quad \tau_E = 100 \frac{m_{final} LHV_{final}}{m_{init} LHV_{init}}, \quad (8)$$

330 where LHV_{final} is the lower heating value of the sample after torrefaction (MJ/kg) and LHV_{init} is
 331 the lower heating value of the sample before torrefaction (MJ/kg). The values of these yields and
 332 of their standard deviations are gathered in Table 2.

333

334 **Table 2**

335 Normalized initial and final masses (%). Torrefaction and energy yields of torrefied HL samples.

Temperature (°C)	Normalized initial mass (g)	Normalized final mass (g)	τ_S Torrefaction yield (%)	τ_E Energy yield %
225 (30 min)	1	0.910±0.004	91.0±0.4	92.7±0.4
250 (30 min)	1	0.891±0.003	89.1±0.3	90.3±0.3
275 (30 min)	1	0.868±0.003	86.8±0.3	87.4±0.3
300 (30 min)	1	0.818±0.003	81.8±0.3	81.4±0.3
225 (60 min)	1	0.900±0.004	90.0±0.4	91.2±0.4
250 (60 min)	1	0.884±0.004	88.4±0.4	89.8±0.5
275 (60 min)	1	0.851±0.003	85.1±0.3	89.5±0.3
300 (60 min)	1	0.782±0.006	78.2±0.6	82.4±0.6

336

337 The torrefaction and energy yields decrease with the isothermal temperature, whatever the
 338 residence time. The decrease of the torrefaction yield is equal to 10% and to 13% between the
 339 samples torrefied at 225 and 300 °C, for the residence times of 30 and 60 minutes, respectively.

340 The decrease of the energy yield is equal to 12% and to 10% between the samples torrefied at

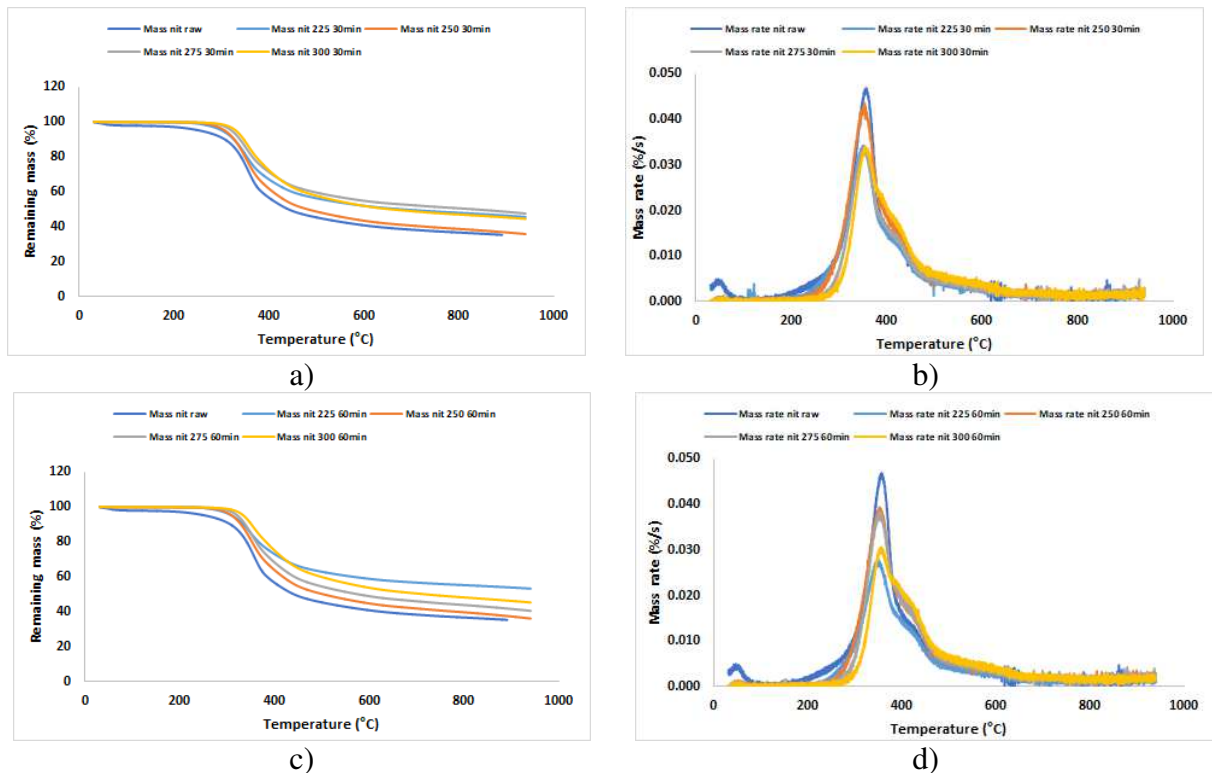
341 225 and 300 °C, for the residence times of 30 and 60 minutes, respectively. In [37], the authors
342 observed similar trends of the torrefaction and energy yields with respect to the isothermal
343 temperature and residence time for microalgal biomass.

344

345 3.2. *Thermogravimetric analyses and kinetic modeling of raw and torrefied HL samples under*
346 *an inert atmosphere (nitrogen) and a heating rate of 5 °C/min*

347 3.2.1 *Thermogravimetric analyses*

348 The mass and mass rate curves of the raw and torrefied materials are gathered in Fig. 2. The
349 masses are expressed in percentages, which have been initialized at 100 at 30 °C, for comparison
350 of the thermodynamic profiles of the different samples in a unique figure.



351 **Fig. 2.** Mass and mass rate curves of non-torrefied (raw) and torrefied (at isothermal
352 temperatures of 225, 250, 275 and 300 °C and during 30 minutes, a) and b), or 60 minutes, c)
353 and d)) HL samples, under nitrogen (nit) and under a heating rate of 5 °C/min.

354

355 The thermogravimetric profiles of the different samples look similar. The mass curves start with
356 a long flat plateau until 200-250 °C. They then present an important decrease until approximately

357 450 °C after which the decrease is much less important. There exist differences between the
358 masses reached at the end of the thermogravimetric experiments. In an unexpected way, the final
359 mass of the sample torrefied at 250 °C is smaller than that of the samples torrefied at other
360 temperatures, especially for the residence time of 30 minutes. The mass rate curve of the raw
361 sample presents a first very small peak before 200 °C, which surely corresponds to the moisture
362 evaporation stage. This small peak does not appear for the torrefied samples, as a consequence of
363 the very low moisture content in these torrefied samples. For all the samples, a much higher peak
364 then appears whose maximum is reached between 350 and 365 °C and which corresponds to the
365 main step of the devolatilization stage. This higher peak presents a shoulder on its left-hand side,
366 whatever the sample, which mainly corresponds to the thermal degradation of the extractives and
367 hemicellulose, as these light molecules are known to decompose at low temperatures. The unique
368 devolatilization peak also presents a large shoulder and a long tail on its right-hand side, which
369 both mainly correspond to the end of the thermal degradation of the lignin part of the sample.
370 Because lignin is an aromatic polymer structure, its decomposition needs higher temperatures to
371 be complete. The differences between the thermodynamic profiles of the raw and torrefied
372 samples essentially lie in the mass reached at the end of the thermogravimetric experiment, in the
373 height of the devolatilization peak and in the importance of the shoulders on the left- and right-
374 hand sides of this devolatilization peak. At the end of the pyrolysis process, the mass rate curves
375 present small oscillations which correspond to the slow degradation of the lignin constituent. For
376 all the samples, the pyrolysis process almost ends at 800 °C, but the mass rate never reaches 0
377 and the mass curves go on slightly decreasing.

378 The shape of the mass rate curves (shoulders, main peak and long tail) obtained for the different
379 samples suggests that four stages may be considered in the pyrolysis process, after the moisture
380 evaporation one.

381 In complement to Fig. 2, some characteristics of these thermal degradations under a non-
382 oxidative atmosphere are indicated in Table 3. The overall temperature range has been split in

383 two subintervals [0,150] and [150,850] (°C) to separate the moisture evaporation and the
 384 devolatilization stages.

385

386 **Table 3**

387 Characteristics of the thermal degradation of the non-torrefied or torrefied (at isothermal
 388 temperature of 225, 250, 275 and 300 °C and during 30 or 60 minutes) HL samples, under
 389 nitrogen and a heating rate of 5 °C/min.

Sample	Temperature range, °C				Total mass loss, %
	30 – 150		150 – 850		
	Mass loss, %	Mass loss, %	Maximal peak temperature, °C	Maximal mass rate, mg/s	
Raw	2.3	61.6	360.2	0.046	63.9
225 °C (30 mn)	0.1	52.6	352.2	0.034	52.7
250 °C (30 mn)	0.1	62.0	357.6	0.042	62.1
275 °C (30 min)	0.1	50.2	350.2	0.033	50.3
300 °C (30 mn)	0.0	53.8	354.0	0.034	53.8
225 °C (60 mn)	0.1	45.3	364.5	0.024	45.4
250 °C (60 mn)	0.3	61.1	355.6	0.039	61.4
275 °C (60 mn)	0.1	57.0	350.2	0.038	57.1
300 °C (60 mn)	0.1	52.6	356.6	0.031	52.7

390

391 The raw HL sample loses 2.3% of its initial mass in the temperature range 30-150 °C due to
 392 moisture evaporation. This moisture evaporation stage leads to the very small peak which
 393 appears in the mass rate curve of the raw sample in the temperature range 30-150 °C, Fig. 2. For
 394 the torrefied samples, the mass losses due to moisture evaporation are almost equal to 0 (mostly
 395 less than 0.1%), because the moisture content of the torrefied samples is much smaller than that
 396 of the raw sample, see Table 1.

397 The devolatilization peak reaches its maximum at quite the same temperature, whatever the
398 sample, between 350.2 and 364.5 °C, with a mean value equal to 356.0 °C. The height of the
399 peak depends on the isothermal torrefaction temperature, this maximal loss rate lying between
400 0.024 and 0.046 %/s, depending on the isothermal torrefaction temperature, but without any clear
401 dependence on this isothermal temperature. The HL samples torrefied at 250 °C present a higher
402 maximal mass rate than that of the samples torrefied at other isothermal temperatures, whatever
403 the torrefaction residence time. They also present higher mass losses and total mass losses, in
404 comparison with the samples torrefied under other experimental conditions.

405

406 *3.2.2. Determination of the kinetic constants through the EIPR model*

407 Because of the presence of the small shoulder on the left-hand side of the devolatilization peak
408 and of a shoulder and of a long tail on the right-hand side of this unique peak, see Fig. 2, at least
409 three constituents (hemicellulose, cellulose and lignin) have to be considered in the EIPR model.
410 But even when considering the raw material and taking the proportions of its constituents as
411 determined through Van Soest's protocol, the simulations returned by the EIPR model with three
412 constituents do not well superimpose with the experimental mass and mass rate curves, whatever
413 the values of the kinetic parameters. Simulations of the pyrolysis of the HL sample torrefied
414 under an isothermal temperature of 300 °C and during 30 minutes have also been performed
415 through the EIPR model considering three constituents, namely hemicellulose, cellulose and
416 lignin, with the fractions 0.09, 0.19 and 0.72, respectively. The mass rate curve simulated with
417 three components does not well reproduce the shoulder and the long tail present of the right-hand
418 side of the main devolatilization peak, see the supplementary material Fig. S1. This may be due
419 to the very high proportion (2/3) of lignin HL samples and because lignin pyrolysis is a complex
420 process as many chemical reactions occur. The mass rate associated to the thermal degradation
421 of lignin under a non-oxidative atmosphere indeed presents peaks at 350 °C from primary
422 pyrolysis reactions, in the range 400–450 °C (methoxyl group-related reactions) and in the range

423 550–600 °C (gasification of catechols (1,2-dihydroxybenzenes)) from secondary pyrolysis
 424 reactions [30,31]. As a consequence, two stages (and only two) in the lignin degradation will be
 425 considered besides that of hemicellulose and cellulose. These two parts of the lignin constituent
 426 will be called lignin1 and lignin2 in the rest of the paper. The extractives will be added to the
 427 hemicellulose and cellulose constituents (half for each). The proportions of these four
 428 constituents of the raw material are deduced from that of extractives, hemicellulose, cellulose
 429 and lignin as determined through Van Soest’s protocol for the raw material and are adjusted from
 430 these proportions for the torrefied samples and according to the previous observations on the
 431 mass and mass rate curves. These proportions are gathered in Table 4.

432

433 **Table 4**

434 Values of the proportions of the four constituents of the HL samples deduced from that of
 435 extractives, hemicellulose, cellulose and lignin as determined through Van Soest’s protocol for
 436 the raw material and adjusted from these proportions for the torrefied samples and observing the
 437 mass and mass rate curves.

	Raw	225 °C 30 min	250 °C 30 min	275 °C 30 min	300 °C 30 min	225 °C 60 min	250 °C 60 min	275 °C 60 min	300 °C 60 min
c _H	0.10	0.06	0.06	0.05	0.04	0.04	0.04	0.04	0.01
c _C	0.23	0.17	0.17	0.17	0.16	0.17	0.16	0.16	0.16
c _{L,1}	0.50	0.50	0.50	0.50	0.50	0.50	0.50	0.50	0.50
c _{L,2}	0.17	0.27	0.27	0.28	0.30	0.29	0.30	0.30	0.33

438

439 The proportions of hemicellulose and cellulose decrease when the isothermal temperature
 440 increases. That of lignin1 has been taken constant, while that of lignin2 increases, as this second
 441 stage of the lignin degradation is supposed to occur at higher temperatures.

442 The optimal values of the kinetic parameters returned by the EIPR model described in section
 443 2.4 and the maximal difference between the experimental and simulated mass rate curves are
 444 gathered in Table 5.

445

446 **Table 5**

447 Optimal values of the kinetic parameters (pre-exponential factors in 1/s and activation energies
 448 in kJ/mol) for the thermal degradation of raw and torrefied samples under a non-oxidative
 449 atmosphere and maximal difference (%/s) between the experimental and simulated mass rate
 450 curves.

	Raw	225 °C 30 min	250 °C 30 min	275 °C 30 min	300 °C 30 min	225 °C 60 min	250 °C 60 min	275 °C 60 min	300 °C 60 min
A _H	8.2E+06	9.2E+06	9.0E+06						
Ea _H	115.0	115.0	115.0	115.0	115.0	115.0	115.0	115.0	115.0
A _C	1.0E+11	1.3E+11	1.2E+11						
Ea _C	161.0	160.0	160.0	160.0	163.0	160.0	160.0	160.0	163.0
A _{L,1}	86.0	101.2	94.4	94.4	95.4	94.4	97.5	94.4	94.4
Ea _{L,1}	60.5	60.5	60.5	60.5	61.7	60.0	60.0	60.0	61.7
A _{L,2}	0.63	0.63	0.64	0.64	0.64	0.64	0.66	0.64	0.64
Ea _{L,2}	43.0	43.0	43.0	43.0	45.0	45.0	45.0	45.0	45.0
Max diff.	1.0E-02	4.0E-03	4.7E-03	4.9E-03	5.0E-03	1.9E-03	3.9E-03	5.9E-03	5.2E-03

451

452 In the worst case (for the raw material), the maximal difference between the experimental and
 453 simulated mass rate curves represents 22% of the maximal height of the mass rate curve. For the
 454 torrefied samples, this maximal difference between the experimental and simulated mass rate
 455 curves represents less than 10% of the maximal height of the mass rate curve. The values of the
 456 kinetic parameters returned by the EIPR model may thus be considered as valid for the pyrolysis
 457 process of the raw and torrefied samples.

458 The values of the optimal activation energies do not vary with the isothermal temperature,
 459 whatever the residence time, except for the cellulose and the lignin1 constituents of the sample
 460 torrefied at 300 °C during 30 or 60 minutes, whose activation energies are slightly higher.

461 In [35], the thermal degradation of raw HL samples has been simulated with the EIPR model but
 462 with another repartition of the constituents of this biomass (for comparison with other woody
 463 biomass or coals considered in this study). The pre-exponential factors were found equal to
 464 1.81×10^4 , 1.06×10^4 and 10.02 1/s for hemicellulose, cellulose and lignin, respectively. The

465 activation energies were found equal to 78.0, 87.0 and 60.0 kJ/mol for hemicellulose, cellulose
 466 and lignin, respectively.

467 In [26], the authors obtained the values of the kinetic parameters gathered in Table 6, using a
 468 DAEM three-component model with an exponent n equal to 1 or greater than 1 in the reaction
 469 function, for Norwegian spruce stump chip. The heating rate was here equal to 40 °C/min.

470

471 **Table 6**

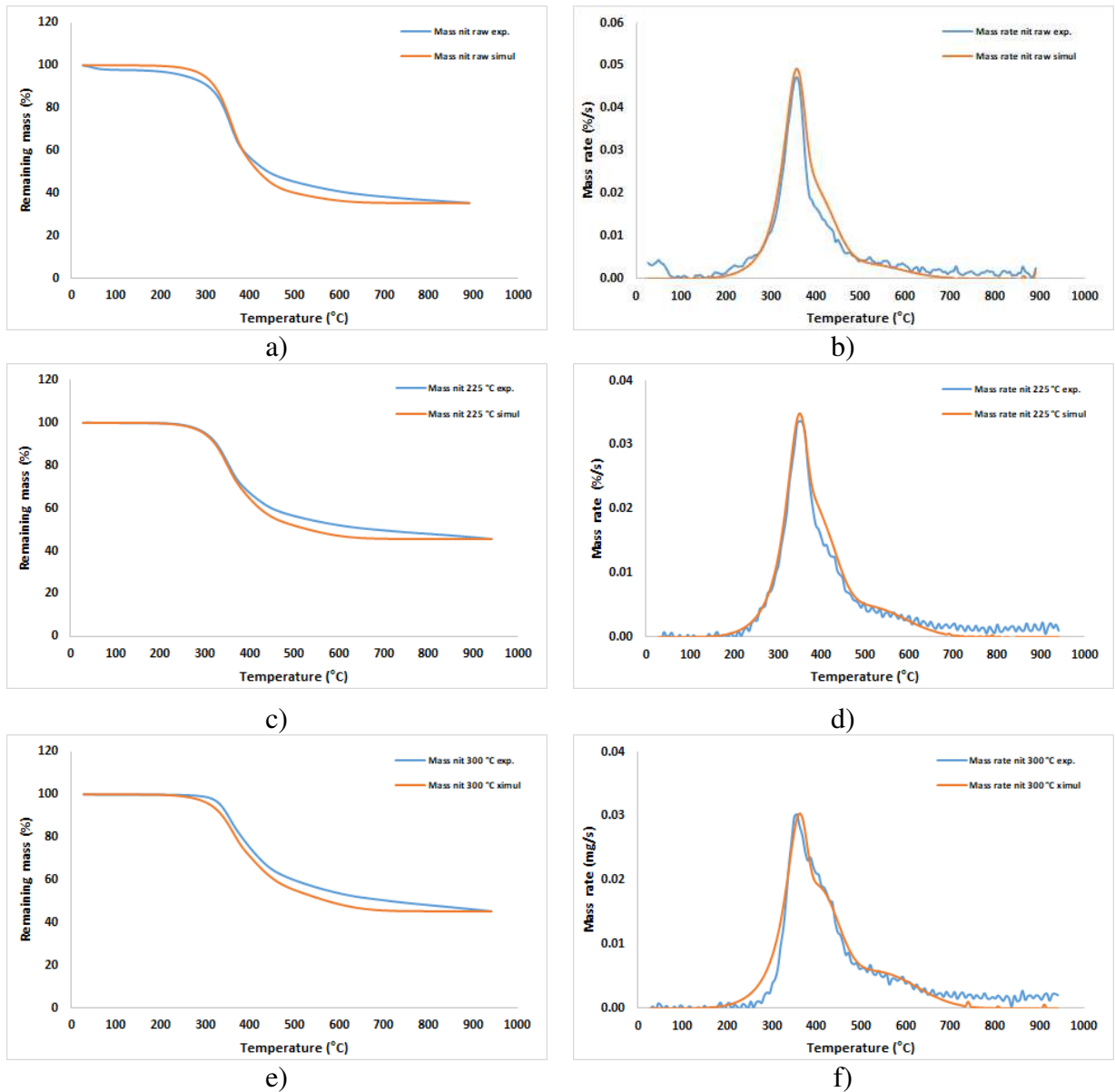
472 Optimal values of the kinetic parameters for torrefied spruce stump samples at three
 473 temperatures (200, 250 and 300 °C) under a heating rate of 40 °C/min. Values of the proportions
 474 of the three constituents (hemicellulose, cellulose and lignin) in the torrefied samples [26].

Sample	n=1			n≠1		
	Ea (kJ/mol)	A (1/s)	c	Ea (kJ/mol)	A (1/s)	c
200 °C	105.36	1.01E+07	0.31	105.13	1.01E+07	0.31
	183.78	3.01E+12	0.54	183.68	3.01E+12	0.55
	40.95	5.54E+00	0.15	58.91	1.33E+02	0.14
250 °C	106.65	1.01E+07	0.21	106.62	1.01E+07	0.21
	182.95	3.01E+12	0.63	182.89	3.01E+12	0.63
	66.73	4.49E+02	0.15	66.18	4.49E+02	0.16
300 °C	-	-	-	-	-	-
	182.33	3.01E+12	0.74	182.32	3.01E+12	0.74
	79.63	3.57E+03	0.26	79.4	3.57E+03	0.26

475

476 In the study [26], the proportions of the three constituents vary with the isothermal temperature,
 477 the hemicellulose being totally degraded after the torrefaction process at 300 °C. Of course, the
 478 study [26] dealing with Norwegian spruce stump chips, the proportions of these constituents are
 479 totally different from that of the HL samples considered in the present study. The activation

480 energies of hemicellulose and lignin are largely comparable to that found in the present study,
 481 the activation energy and the pre-exponential factor of cellulose being slightly higher in [26]
 482 than in the present study.
 483 The experimental and simulated mass and mass rate of the raw material, of the torrefied material
 484 at 225 °C during 30 minutes and of the torrefied material at 300 °C during 60 minutes are
 485 gathered in Fig. 3.



486 **Fig. 3.** Experimental (blue) and simulated (red) mass and mass rate curves for raw sample a) and
 487 b), or torrefied sample at 225 °C during 30 minutes c) and d), or torrefied sample at 300 °C and
 488 during 60 minutes e) and f), under a non-oxidative atmosphere and a heating rate of 5 °C/min.

489

490 The simulated mass and mass rate curves quite well superimpose with the experimental ones,
491 even if the simulated mass rate curve fails to start very abruptly on the left-hand side of the
492 devolatilization peak for the sample torrefied at 300 °C during 60 minutes. This failure is
493 responsible for the quite high maximal differences observed in Table 5. The simulated mass rate
494 curves reach 0 after 750 °C, while the experimental ones go on oscillating, because of the slow
495 degradation of the lignin constituent. But the overall shape of the mass and mass rate curves is
496 quite well reproduced in these simulations and especially the previously described four stages of
497 the devolatilization process.

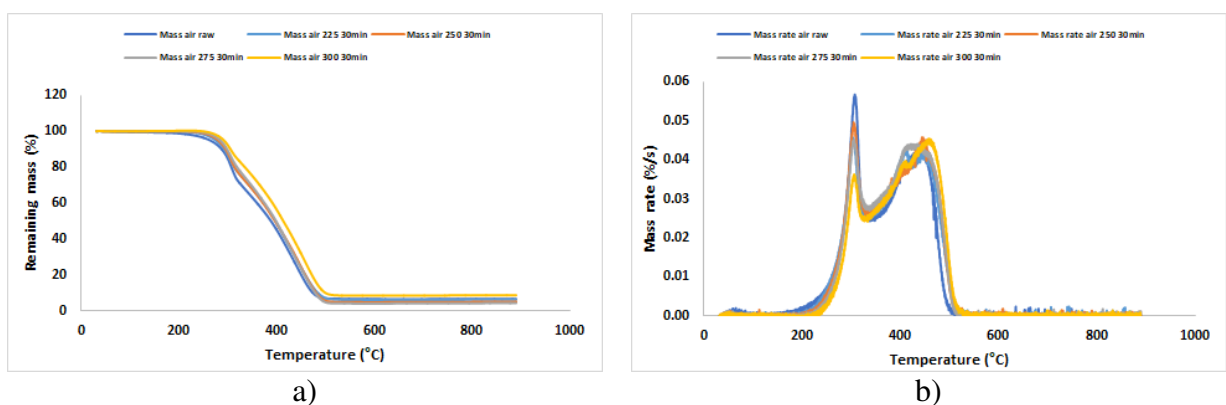
498 The simulations of the thermal degradation of the other samples present very similar trends in
499 comparison to that of the ones presented in Fig. 3 and will not be presented.

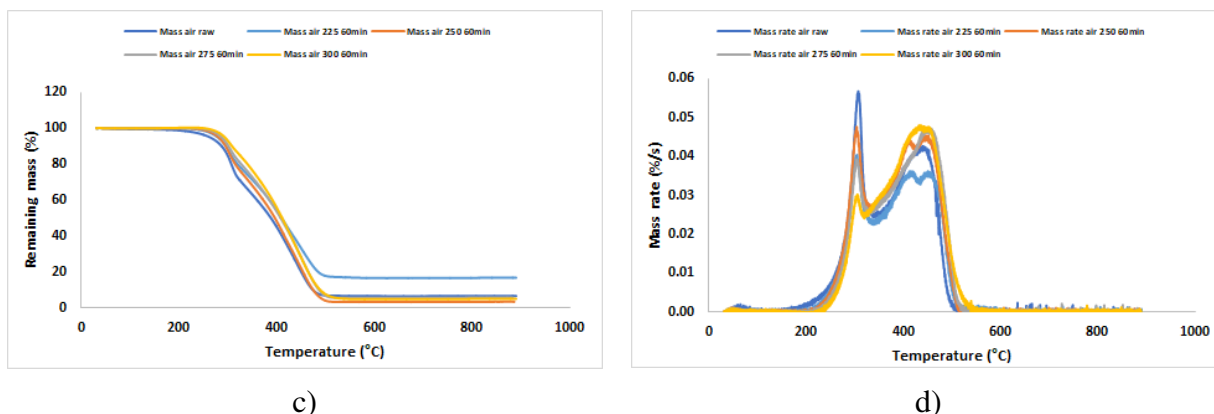
500

501 *3.3 Thermogravimetric analyses and kinetic modeling of raw and torrefied HL samples*
502 *under an oxidative atmosphere (synthetic air) and under a heating rate of 5 °C/min*

503 *3.3.1 Thermogravimetric analyses*

504 The mass and mass rate curves of the raw and torrefied samples are gathered in Fig. 4. The
505 masses are expressed in percentages, which have been initialized at 100 at 30 °C, for comparison
506 of the thermodynamic profiles of the different samples in a unique figure.





507 **Fig. 4.** Mass and mass rate curves of raw and torrefied (at isothermal temperatures of 225, 250,
 508 275 and 300 °C and during 30 minutes a) and b), or during 60 minutes c) and d)) HL samples,
 509 under an oxidative atmosphere (air) and a heating rate of 5 °C/min.

510

511 A very small peak occurs on the mass rate curve of the raw material in the temperature range 30-
 512 150 °C, which corresponds to the moisture evaporation. This small peak does not appear for the
 513 torrefied samples, as a consequence of the very low moisture content in these samples.

514 The thermal degradation profiles of the different samples under air look very similar. A first long
 515 and flat plateau first appears on the mass curves which ends at around 200 °C. Then the mass
 516 starts decreasing with a possible change of the decreasing rate at around 300 °C. The mass
 517 curves end with a flat plateau, but the height of this plateau (final mass of the sample) depends
 518 on the isothermal temperature. On the mass rate curves, a first thin peak appears at around 307
 519 °C, whatever the sample, which mainly corresponds to the thermal degradations of the
 520 hemicellulose, cellulose and part of the lignin constituents, through a devolatilization process. A
 521 second thicker peak occurs at around 450 °C which corresponds to the char combustion. The
 522 changes in the mass rate curves mainly concern the height of the devolatilization and combustion
 523 peaks. Again small oscillations appear at the end of the mass rate curves which correspond to the
 524 end of the slow degradation of the lignin. After 650 °C, the mass curves exhibit a flat plateau
 525 which means that the sample mass does not evolve so much at these higher temperatures. For all
 526 the samples, the thermal degradation thus ends before 650 °C, which is lower than the end of the
 527 pyrolysis process. Oxygen is known to enhance the degradation process.

528 In complement to Fig. 4, some characteristics of the different mass and mass rate curves are
 529 gathered in Table 7 for the different samples. Again, the overall temperature range has been split
 530 in two subintervals [0,150] and [150,850] (°C) to separate the moisture evaporation and the
 531 devolatilization stages.

532

533 **Table 7**

534 Characteristics of the mass and mass rate curves of the raw or torrefied (at isothermal
 535 temperatures of 225, 250, 275 or 300 °C and during 30 or 60 minutes) HL samples, under an
 536 oxidative atmosphere and a heating rate of 5 °C/min.

	Temperature range						Total mass loss, %
	30 -150 °C		150 – 850 °C				
	Mass loss, %	Maximum peak 1 temp. °C	Maximal mass rate 1, %/s	Maximum peak 2 temp. °C	Maximal mass rate 2, %/s	Mass loss %	
Raw	0.7	309.1	0.056	449.2	0.042	92.6	93.3
225 °C (30 min)	0.1	309.0	0.042	447.3	0.041	93.5	93.6
250 °C (30 min)	0.1	309.6	0.046	446.3	0.046	94.8	94.9
275 °C (30 min)	0.0	305.1	0.045	447.0	0.043	95.6	95.6
300 °C (30 min)	0.0	307.4	0.036	449.7	0.045	91.2	91.2
225 °C (60 min)	0.1	305.3	0.040	449.0	0.036	83.0	83.1
250 °C (60 min)	0.1	304.3	0.048	448.6	0.045	96.4	96.5
275 °C (60 min)	0.0	305.1	0.039	449.2	0.047	94.2	94.2
300 °C (60 min)	0.0	305.7	0.030	449.3	0.047	94.9	94.9

537

538 The mass loss associated to the moisture evaporation of the raw HL sample is equal to 0.7%.
 539 Concerning the samples torrefied during 30 or 60 minutes, the moisture evaporation phase which
 540 occurs before 150 °C leads to very small mass losses, less than 0.1%. The mass rate curves of the
 541 torrefied samples thus do not present a similar peak in this temperature range.
 542 The temperature at which this first peak occurs lies in the range 304.3-309.6 °C, with a mean
 543 value of 306.4 °C. The temperature at which the second peak occurs lies in the range 447.0-

544 449.3 °C, with a mean value of 448.4 °C. It should be observed that the maximal mass rate of the
 545 first peak decreases and that of the second peak increases with the isothermal temperature. This
 546 is the consequence of an increasing degradation of the light molecules contained in the samples
 547 when the isothermal temperature increases.

548

549 3.3.2 Determination through the EIPR model of the kinetic parameters

550 Four constituents of the HL samples will again be considered, namely hemicellulose, cellulose,
 551 lignin1 and lignin2 (apart from the moisture which is almost negligible in the present case), even
 552 if the four stages of the devolatilization process do not clearly appear on the mass rate curves of
 553 Fig. 4. The fraction c_i of each constituent is taken from Table 4 for each sample.

554 The values of the parameters $\tau_{vol,i}$ for the four constituents of the samples, the optimal values of
 555 the kinetic parameters returned by the EIPR model described in section 2.5 and the maximal
 556 difference between the experimental and simulated mass rate curves are gathered in Table 8.

557

558 **Table 8**

559 Fractions $\tau_{vol,i}$ of volatiles contained in the constituents. Optimal values of the kinetic
 560 parameters (pre-exponential factors in 1/s (or in 1/s·Pa for A_{comb}) and activation energies in
 561 kJ/mol) for the thermal degradation of raw and torrefied samples under an oxidative atmosphere
 562 and maximal difference (error, in %/s) between the experimental and simulated mass rate curves.

	Raw	225 °C	250 °C	275 °C	300 °C	225 °C	250 °C	275 °C	300 °C
		30 min	30 min	30 min	30 min	60 min	60 min	60 min	60 min
$\tau_{vol,1}$	0.80	0.70	0.70	0.70	0.70	0.70	0.70	0.70	0.70
$\tau_{vol,2}$	0.80	0.70	0.70	0.70	0.70	0.70	0.70	0.70	0.70
$\tau_{vol,3}$	0.35	0.25	0.25	0.25	0.25	0.25	0.25	0.25	0.25
$\tau_{vol,4}$	0.35	0.25	0.25	0.25	0.25	0.25	0.25	0.25	0.25
A_H	5.2E+06	5.2E+06	5.0E+06	5.2E+06	5.2E+06	5.2E+06	5.2E+06	5.2E+06	5.2E+06

Ea _H	99.0	97.0	97.0	97.0	97.0	97.0	97.0	97.0	97.0
A _C	1.0E+12	1.0E+12	1.0E+12	9.0E+11	1.0E+12	1.0E+12	1.0E+12	1.0E+12	1.0E+12
Ea _C	161.0	160.0	160.0	160.0	160.0	160.0	160.0	160.0	163.0
A _{L,1}	95.0	95.0	87.1	95.3	95.0	95.0	95.1	87.8	97.0
Ea _{L,1}	64.0	62.0	63.0	63.0	64.0	62.0	62.0	64.0	67.0
A _{L,2}	95.0	95.0	95.0	95.0	95.0	95.0	95.0	97.0	97.0
Ea _{L,2}	64.0	62.0	63.0	63.0	64.0	62.0	62.0	64.0	67.0
A _{comb}	1.9E-02	9.8E-03	9.0E-03	1.0E-02	1.0E-02	1.0E-02	9.9E-03	1.5E-02	1.5E-02
Ea _{comb}	73.0	69.5	69.5	69.5	70.0	69.5	69.5	73.0	73.0
Max.diff.	1.2E-02	9.6E-03	1.6E-02	1.1E-02	1.1E-02	8.6E-03	1.1E-02	1.1E-02	1.2E-02

563

564 The $\tau_{vol,i}$ parameters are taken independent of the torrefaction conditions but they depend on the
565 constituents.

566 The activation energies of the four constituents do not really vary with respect to the isothermal
567 temperature and to the residence time, except for the raw sample and for the samples torrefied at
568 275 and 300 °C, for which a small increase of the activation energies appears.

569 In [38], the authors performed a kinetic modeling of raw and torrefied Norwegian spruce. In the
570 case of dry torrefaction, the spruce sample were submitted to an isothermal temperature of 275
571 °C during 60 minutes under an inert atmosphere. For the kinetic modeling, the authors used a
572 three pseudo-component model. The values of the optimal kinetic parameters they obtained are
573 gathered in the Table 9.

574

575 **Table 9**

576 Optimal values of the kinetic parameters (A in 1/s, Ea in kJ/mol), proportions of the three
577 constituents of the raw and torrefied spruce samples. Values of the reaction order n . From [38].

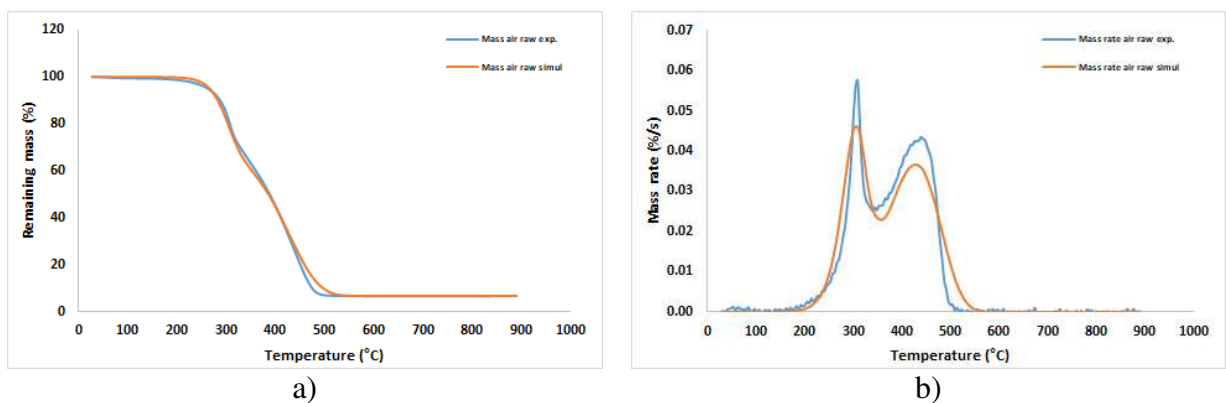
Sample	Hemicellulose	Cellulose	Lignin	Char
--------	---------------	-----------	--------	------

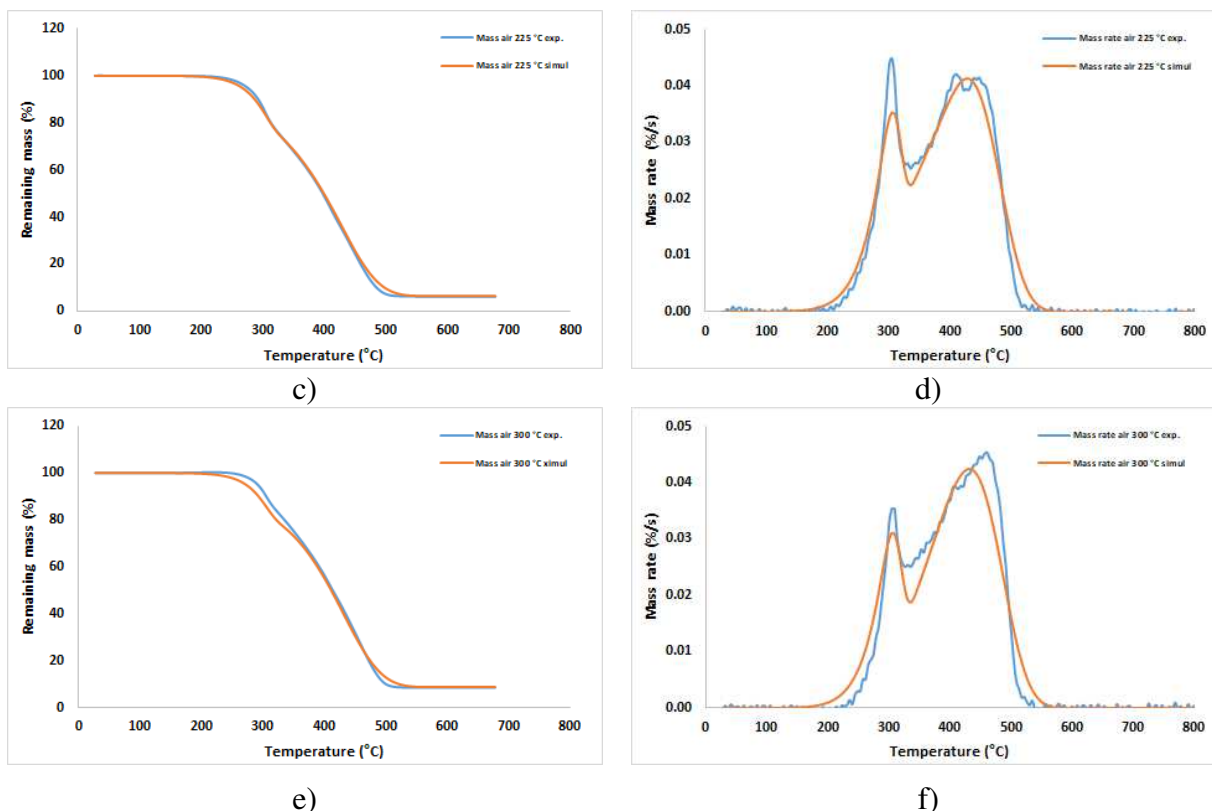
Raw	Ea	103.80	221.58	66.17	178.48
	A	3.70×10^7	2.43×10^{17}	1.33×10^3	5.92×10^{10}
	c	0.14	0.42	0.23	0.21
	n	1	1	1	1.01
Dry torrefaction at 275 °C during 60 minutes	Ea	-	237.78	72.78	202.75
	A	-	1.32×10^{19}	4.25×10^3	3.12×10^{12}
	c	-	0.36	0.30	0.34
	n	-	1	1	1.01

578

579 In the study [38], the hemicellulose part of the spruce sample has totally disappeared after the
 580 torrefaction performed at 275 °C during 60 minutes. The values of the pre-exponential factors
 581 and of the activation energies of cellulose, lignin and char significantly increase for the torrefied
 582 sample when compared to that of the raw sample. These values are much higher than that
 583 returned by the EIPR model in the case of HL samples considered in the present study. But the
 584 compositions of the materials are totally different.

585 The experimental and simulated mass and mass rate of the raw sample, of the torrefied sample at
 586 225 °C during 30 minutes and of the torrefied sample at 300 °C during 60 minutes are gathered
 587 in Fig. 5.





588 **Fig. 5.** Experimental (blue) and simulated (red) mass and mass rate curves of the raw sample a)
 589 and b), of the torrefied sample at 225 °C during 30 minutes c) and d), or the torrefied sample at
 590 300 °C and during 60 minutes e) and f), under an oxidative atmosphere and a heating rate of 5
 591 °C/min.

592

593 The simulated mass and mass rate curves quite well superimpose with the experimental ones, see
 594 also the maximal differences indicated in Table 8.

595 The simulations of the thermal degradation of the other samples look very similar to the ones
 596 presented in Fig. 5 and will not be presented.

597 Again the torrefaction process under the conditions of the present study do not highly alter the
 598 constituents of the hydrolysis sample.

599

600 **4. Conclusion**

601 Russian hydrolysis lignin samples from Onega dump were torrefied in a fixed bed reactor under
 602 a non-oxidative atmosphere at isothermal temperatures of 225, 250, 275 or 300 °C, during 30 or

603 60 minutes. The impact of these different torrefaction conditions was analyzed through
604 thermogravimetric analyses performed under non-oxidative or oxidative atmospheres and under
605 a heating rate of 5 °C/min from ambient temperature to 900 °C. The shapes of the mass rate
606 curves of the raw and torrefied samples look quite similar under each atmosphere, the differences
607 being essentially associated to the final mass and to the maximal mass rate. The values of the
608 kinetic parameters of the different samples were determined using the EIPR model with four
609 constituents in each material (hemicellulose, cellulose and two stages of the lignin degradation).
610 The variations of these values did not vary in a significant way with respect to the isothermal
611 temperature or torrefaction residence time. Torrefying HL samples under the lowest isothermal
612 temperature (200 °C) and during the shortest residence time (30 minutes) thus seems to be
613 enough to obtain a valuable combustible. This torrefied sample has indeed a lower moisture
614 content, a higher carbon content and higher calorific value. The torrefaction process performed
615 under this low temperature does not degrade in a significant way the hydrolysis lignin sample.
616
617 This research did not receive any specific grant from funding agencies in the public, commercial,
618 or not-for-profit sectors.

619

620

621 Nomenclature

A	Pre-exponential factor, 1/s	I	Number of constituents to be taken into account
Ea	Activation energy, kJ/mol	J	Number of experimental time points (J is approximately equal to 200)
c_i	Mass fraction of the constituent i	LHV	Lower Heating Value
$\left(\frac{dm_{vol,i}^e}{dt}\right)_{exp}(t_j)$	Experimental mass rate at time t_j , %/s	$m_{vol,i}^e$	Mass of volatiles emitted from the constituent i at time t , %
$\left(\frac{dm_{vol,i}^e}{dt}\right)_{sim}(t_j)$	Simulated mass rate at time t_j , %/s	$m_{char,i}^c$	Mass of char from the constituent i consumed at time t , %

$\left(\frac{dm_{char,i}^c}{dt}\right)_{exp}(t_j)$	Experimental char mass rate at time t_j , %/s	$m_i(0)$	Initial mass of the constituent i , %
$\left(\frac{dm_{char,i}^c}{dt}\right)_{sim}(t_j)$	Simulated char mass rate at time t_j , %/s	P_{O_2}	Oxygen pressure, Pa
EIPR	Extended Independent Parallel Reaction	R	Ideal gas constant, J/mol K
f	Reaction function	t	Time parameter, s
HL	Hydrolysis lignin	T	Temperature, K
$\tau_{vol,i}$	Fraction of volatiles contained in the constituent i	α	Extent of conversion

622

623 **References**

- 624 [1] Abbasi T, Abbasi SA. Biomass energy and the environmental impacts associated with its
625 production and utilization. *Renew Sustain Energy Rev* 2010;14:919-37.
626 doi:10.1016/j.rser.2009.11.006.
- 627 [2] Goldfarb JL, Liu C. Impact of blend ratio on the co-firing of a commercial torrefied biomass
628 and coal via analysis of oxidation kinetics. *Bioresour Technol* 2013;149:208-15.
629 <http://dx.doi.org/10.1016/j.biortech.2013.09.053>
- 630 [3] Rabinovich ML, Fedoryak O, Dobeles G, Andersone A, Gawdzik B, Lindstrom ME,
631 Sevastyanova O. Carbon adsorbents from industrial hydrolysis lignin: The USSR/Eastern
632 European experience and its importance for modern biorefineries. *Renew Sustain Energy Rev*
633 2016;57:1008–24. <http://dx.doi.org/10.1016/j.rser.2015.12.206>.
- 634 [4] Rabinovich ML. Lignin by-products of soviet hydrolysis industry: resources, characteristics,
635 and utilization as a fuel. *Cellulose Chem Technol* 2014;48(7-8);613-31.
- 636 [5] Mahmood N, Yuan Z, Schmidt J, Tymchyshyn M, Xu C. Hydrolytic liquefaction of
637 hydrolysis lignin for the preparation of bio-based rigid polyurethane foam. *Green Chemistry*
638 2016;18:2385-98. DOI 10.1039/C5GC02876K.
- 639 [6] Bach QV, Skreiberg O. Upgrading biomass fuels via wet torrefaction: A review and
640 comparison with dry torrefaction. *Renew Sustain Energy Rev* 2016;54:665-77.
641 <http://dx.doi.org/10.1016/j.rser.2015.10.014>.

- 642 [7] Bergman PCA, Boersma AR, Zwart RWR, Kiel JHA. Torrefaction for biomass co-firing in
643 existing coal-fired power stations: BIOCOAL. ECN report. Renewable energy in the
644 Netherlands. 2005;ECN-C-05-013.
- 645 [8] Van der Stelt MJC, Gerhauser H, Kiel JHA, Ptasiński KJ. Biomass upgrading by torrefaction
646 for the production of biofuels: a review. *Biomass Bioenergy* 2011;35(9):3748-62.
647 <http://doi.org/10.1016/j.biombioe.2011.06.023>.
- 648 [9] Koppejan J, Sokhansank S, Jess J, Wright C, Boardman R. Status overview of torrefaction
649 technologies. 2012 Enschede: International Energy Agency (IEA).
- 650 [10] Eseltine D, Thanapal SS, Annamalai K, Ranjan D. Torrefaction of woody biomass (Juniper
651 and Mesquite) using inert and non-inert gases. *Fuel* 2013;113:379-88.
652 <http://dx.doi.org/10.1016/j.fuel.2013.04.085>.
- 653 [11] Wannapeera J, Fungtammasan B, Worasuwanarak N. Effects of temperature and holding
654 time during torrefaction on the pyrolysis behaviors of woody biomass. *J Anal Appl Pyrol*
655 2011;92:99-105.
- 656 [12] Rousset P, Macedo L, Commandré JM, Moreira A. Biomass torrefaction under different
657 oxygen concentrations and its effect on the composition of the solid by-product. *J Anal Appl*
658 *Pyrol* 2012;96:86-91.
- 659 [13] Li H, Liu X, Legros R, Bi XT, Lim CJ, Sokhansanj S. Torrefaction of sawdust in a fluidized
660 bed reactor, *Bioresour Technol* 2012;103:453-458. doi:10.1016/j.biortech.2011.10.009
- 661 [14] Tumuluru JS, Wright CT, Hess JR, Kenney KL. A review of biomass densification systems
662 to develop uniform feedstock commodities for bioenergy application. *Biofuels Bioproducts*
663 *Biorefining* 2011;5(6):683-707. DOI:10.1002/bbb.324.
- 664 [15] Magdziarz A, Wilk M, Straka R. Combustion process of torrefied wood biomass. *J Thermal*
665 *Anal Calor* 2017;127:1339-49 DOI 10.1007/s10973-016-5731-0.

666 [16] Chen WH, Kuo PCh. A study on torrefaction of various biomass materials and its impact on
667 lignocellulosic structure simulated by thermogravimetry. *Energy* 2010;35:2580-86.
668 <https://doi.org/10.1016/j.energy.2010.02.054>.

669 [17] Chen WH, Kuo PCh. Isothermal torrefaction kinetics of hemicellulose, cellulose, lignin and
670 xylan using thermogravimetric analysis. *Energy* 2011;36:6451-60.
671 [doi:10.1016/j.energy.2011.09.022](https://doi.org/10.1016/j.energy.2011.09.022)

672 [18] Uslu A, Faaij APC, Bergman PCA. Pre-treatment technologies, and their effect on
673 international bioenergy supply chain logistics. Techno-economic evaluation of torrefaction, fast
674 pyrolysis and pelletisation. *Energy* 2008;33(8):1206-23.
675 <https://doi.org/10.1016/j.energy.2008.03.007>.

676 [19] Adams PWR, Shirley JEJ, Whittaker C, Schield I, Darvell LI, Jones JM, McManus MC.
677 Integrated assessment of the potential for torrefied wood pellets in the UK electricity market. In:
678 World bioenergy 2014 conference, 2014 Jönköping, Sweden.

679 [20] Adams PWR, Shirley JEJ, McManus MC. Comparative cradle-to-grate life cycle
680 assessment of wood pellet production with torrefaction. *Appl Energy* 2015;138:367-80.
681 <https://doi.org/10.1016/j.apenergy.2014.11.002>.

682 [21] National Non-Food Crops Centre (NNFCC). Techno-economic assessment of biomass
683 densification technologies. Project 08-015. 2008 York.

684 [22] Jarvinen T, Agar, D. Experimentally determined storage and handling properties of fuel
685 pellets made from torrefied whole-tree pine chips, logging residues and beech stem wood. *Fuel*
686 2014;129:330-39. <https://doi.org/10.1016/j.fuel.2014.03.057>.

687 [23] Stelte W, Sanadi AR, Shanf L, Holm JK, Ahrenfeldt J, Henrikson UB. Recent developments
688 in biomass pelletisation – a review. *BioResources* 2012;7(3):4451-90.

689 [24] Martín-Lara MA, Ronda A, Zamora MC, Calero M. Torrefaction of olive tree pruning:
690 Effect of operating conditions on solid product properties. *Fuel* 2017;202:109–17.
691 <http://dx.doi.org/10.1016/j.fuel.2017.04.007>

692 [25] Talero G, Rincon S, Gomez A. Torrefaction of oil palm residual biomass:
693 Thermogravimetric characterization. *Fuel* 2019;242:496–506.
694 <https://doi.org/10.1016/j.fuel.2019.01.057>

695 [26] Tran KQ, Bach QV, Trinh TT, Seisenbaeva G. Non-isothermal pyrolysis of torrefied stump
696 – A comparative kinetic evaluation. *Appl Energy* 2014;136:759–66.
697 <http://dx.doi.org/10.1016/j.apenergy.2014.08.026>

698 [27] Barskov S, Zappi M, Buchireddy P, Dufreche S, Guillory J, Gang D, Hernandez R, Bajpai
699 R, Baudier J, Cooper R, Sharp R. Torrefaction of biomass: A review of production methods for
700 biocoal from cultured and waste lignocellulosic feedstocks. *Renew Energy* 2019;142:624-642.
701 <https://doi.org/10.1016/j.renene.2019.04.068>.

702 [28] Chew JJ, Doshi V. Recent advances in biomass pretreatment – Torrefaction fundamentals
703 and technology. *Renew Sustain Energy Rev* 2011;15:4212–22. doi:10.1016/j.rser.2011.09.017

704 [29] Chen WH, Peng J, Bi XT. A state-of-the-art review of biomass torrefaction, densification
705 and applications. *Renew Sustain Energy Rev* 2015;44:847–66.
706 <http://dx.doi.org/10.1016/j.rser.2014.12.039>.

707 [30] Jiang X, Lu Q, Hu B, Liu J, Dong C, Yang Y. Intermolecular interaction mechanism of
708 lignin pyrolysis: A joint theoretical and experimental study. *Fuel* 2018;215:386–94.
709 <https://doi.org/10.1016/j.fuel.2017.11.084>.

710 [31] Kawamoto H. Lignin pyrolysis reactions. *J Wood Sci* 2017;63:117–32. DOI
711 10.1007/s10086-016-1606-z.

712 [32] Van Soest PJ, Robertson JB, Lewis BA. Methods for Dietary Fiber, Neutral Detergent
713 Fiber, and Nonstarch Polysaccharides in Relation to Animal Nutrition, *J Dairy Sci*
714 1991;74:3583–97. doi:10.3168/jds.S0022-0302(91)78551-2.

715 [33] Damartzis T, Vamvuka D, Sfakiotakis S, Zabaniotou A, Thermal degradation studies and
716 kinetic modeling of cardoon (*Cynara cardunculus*) pyrolysis using thermogravimetric analysis
717 (TGA), *Bioresour Technol* 2011;102:6230-38. <https://doi.org/10.1016/j.biortech.2011.02.060>.

718 [34] Sfakiotakis S, Vamvuka D. Development of a modified independent parallel reactions
719 kinetic model and comparison with the distributed activation energy model for the pyrolysis of a
720 wide variety of biomass fuels, *Bioresour Technol* 2015;197:434–42.
721 <http://dx.doi.org/10.1016/j.biortech.2015.08.130>

722 [35] Popova E, Chernov A, Maryandyshev P, Brillard A, Kehrli D, Trouvé G, Lyubov V, Brillhac
723 JF. Thermal degradation of wood biofuels, coals and hydrolysis lignin from the Russian
724 Federation: Experiments and modelling. *Bioresour Technol* 2016;218:1046-54.
725 <http://dx.doi.org/10.1016/j.biortech.2016.07.033>.

726 [36] Brillard A, Brillhac JF. Improvements of global models for the determination of the kinetic
727 parameters associated to the thermal degradation of lignocellulosic materials under low heating
728 rates. *Renew Energy* 2020;146:1498e1509. <https://doi.org/10.1016/j.renene.2019.07.040>

729 [37] Zhang C, Wang C, Cao G, Chen WH, Ho SH. Comparison and characterization of property
730 variation of microalgal biomass with non-oxidative and oxidative torrefaction, *Fuel*
731 2019;246:375–85. <https://doi.org/10.1016/j.fuel.2019.02.139>

732 [38] Bach QV, Tran KQ. Dry and wet torrefaction of woody biomass – A comparative study on
733 combustion kinetics. *Energy Procedia* 2015;75 :150–55. doi: 10.1016/j.egypro.2015.07.270.